HiSST: 3rd International Conference on
High-Speed Vehicle Science Technology
14 -19 April 2024, Busan, Korea

Numerical aero-shape characterization of an Inflatable Heat Shield re-entry vehicle in the EFESTO-2 project.

Y.Prevereaud[1], Y.Dauvois[2], J.Zhai[3], T.Gawehn[4], G.Guidotti[5], G.Governale[6]

Abstract

Inflatable Heat Shields (IHS) are considered as a breakthrough solution to support realization of innovative re-entry space missions as a significant increase of payload capability and space systems recovery. For this solution to become operational, a number of key technologies must be matured towards an appropriate level. In the frame of the European EFESTO-2 project, structural and aerodynamic ground tests are planned to improve knowledge of this peculiar inflatable aerodynamic decelerator system. To reach this goal, a numerical study is carried out to simulate the maximum expected deformation level of the heat shield during the re-entry. Then, undeformed and deformed shapes of the heat shield are tested in the H2K and TMK wind tunnels, followed by post-test numerical rebuilding. This paper presents pre-numerical investigation pointing out the definition of the test articles and the test campaigns, as well as post numerical rebuilding of TMK test experiments with numerical-experimental cross-checks.

Keywords: *inflatable heat shields, hypersonic re-entry aerodynamics and aerothermodynamics, wind-tunnel testing, numerical rebuilding, fluid-structure interaction*

Nomenclature

Computational Fluid Dynamic (CFD)
Finite Element Method (FEM)
Flexible TPS (F-TPS)
Fluid Structure Interaction Loop (FSI)
Inflatable Heat Shield (IHS)
Inflatable Structure (IS)
Thermal Protection System (TPS)
Technology Readiness Level (TRL)
Wind Tunnel Test (WTT)

1. EFESTO-2 project set-up

1.1. EFESTO-2 objectives

Inflatable Heat Shields (IHS) are considered as a breakthrough solution to support realization of innovative re-entry space missions for both increasing significantly payload capability and space systems recovery. For this solution to become operational, a number of key technologies must be matured to an appropriate readiness level and that's what is being done in Europe through the projects EFESTO [1-3] and EFESTO-2 [1, 4-8], respectively under the programs H2020 (grant No. 821801) and HORIZON EUROPE (grant No. 1010811041). EFESTO-2 project is managed by a European consortium,

[1] *ONERA/DMPE, Université de Toulouse, F-31055 Toulouse – France,* ysolde.prevereaud@onera.fr
[2] *ONERA/DMPE, Université de Toulouse, F-31055 Toulouse – France,* yann.dauvois@onera.fr
[3] *German Aerospace Center (DLR), Supersonic and Hypersonic Technologies, Köln, Germany,* Junnai.Zhai@dlr.de
[4] *German Aerospace Center (DLR), Supersonic and Hypersonic Technologies, Köln, Germany,* Thomas.Gawehn@dlr.de
[5] *Deimos Space S.L.U, Tres Cantos 28760, Spain,* giuseppe.guidotti@deimos-space.com,
[6] *Politecnico di Torino, Department of Mechanical and Aerospace Engineering, Turin – Italy,* giuseppe.governale@polito.it

coordinated by Deimos Space (ES), and including CIRA (IT), DEIMOS ENGHENARIA (PT), DLR (DE), ONERA (FR), PANGAIA-GRADO-ZERO (IT) and POLITO (IT). This project is run through four main macro-tasks as follows: a business case analysis, a reference mission and system engineering, an extensive ground testing and eventually near-future activities identification.

Based on a Business Case analysis, a reference study-case for a baseline application (see Fig 1) is selected and a design loop is then executed to define the mission envelope and to derive the system mechanical and thermal sizing of a re-entry vehicle with an integrated inflatable heat shield.

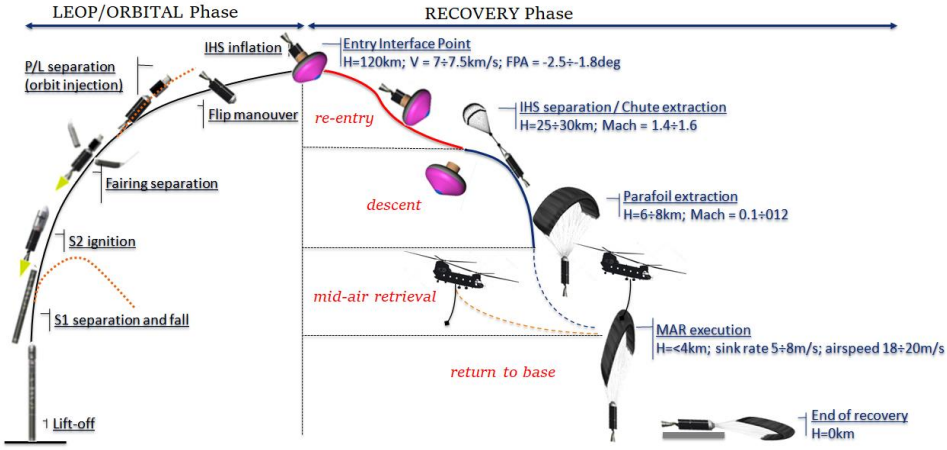

Fig 1. EFESTO-2 ConOps and system configuration.

In the EFESTO-2 project, a particular focus is dedicated to aero-shape investigation, in terms of aerodynamics and aerothermodynamics optimization, including numerical and experimental efforts. The objective is to evaluate the influence of the heat-shield deformation on the aerothermodynamic parameters.

To address this goal, a numerical study is carried out to determine the maximum expected deformation level of the heat shield during the re-entry and to quantify the influence of this deformation on the aerothermodynamic coefficients. Based on these data, undeformed and deformed shape models are designed and tested in the DLR H2K and TMK wind tunnels for the evaluation of both static and dynamic stabilities. Then, a numerical rebuilding of the wind-tunnel tests is achieved to calibrate numerical models, to update and consolidate the aerodynamic database and to enhance the flying quality assessment. This paper presents a pre-numerical investigation allowing the definition of the test articles and the test campaigns, as well as post numerical rebuilding of the TMK tests within a numerical-experimental cross-checking process. The wind tunnel test campaigns are displayed in a separate paper, where details can be found [7].

1.2. Aerothermodynamic characterization of the (un)deformed IHS

The aeroshape characterization of the EFESTO-2 IHS encompasses the whole loop from numerical simulation with CFD, to experimental investigation through wind-tunnel testing, and finally with cross-check between numerical and experimental results to update the aero-database set (see Fig 2).

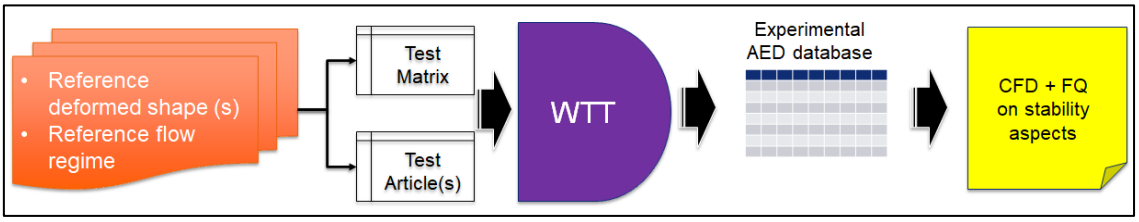

Fig 2. Aerodynamic experimental and numerical investigation.

The process includes the following steps: 1) Aerodynamic and aerothermodynamic analysis of the reference undeformed shape; 2) Fluid structure interaction analysis to define the maximum level of

deformation; 3) Wind-tunnel tests; 4) WTT-CFD Cross-check to evaluate uncertainties associated to numerical simulation. These uncertainties are then reported into the aerodynamic database to consolidate the mission and system design.

2. Analysis of the aerodynamic and aerothermodynamic of EFESTO-2 undeformed aero-shape

2.1. Undeformed aero-shape design and trajectory

Based on EFESTO-1 heritage, different aero-shape variants have been investigated and traded against each other in order to satisfy all the defined requirements: Length/Diameter ratio, flight path angle, ballistic coefficient, half-cone angle, and aerodynamic / aerothermodynamic assessments associated to each entry corridor explored [5]. The aerodynamic and aerothermodynamic database are firstly built with the ONERA engineering code ARES, allowing fast simulations along fully trajectories or for selected flight conditions. The associated uncertainties are estimated by cross-comparison with CFD results at specific chosen conditions.
Finally, the chosen aero-shape, illustrated in Fig 3, is a 60° half-angle blunted-cone with a spherical nose of 1.3 m radius and an elliptical annulus for a total size of 5.32 m diameter, featuring a front surface of 22.21 m². Compared to the previous EFESTO-1 geometry, the EFESTO-2 aero-shape update permits a reduction of the mass system to 1600 kg, and thus a significant cost saving. Various entry trajectories are defined: a *Reference trajectory* and two *Sizing trajectories* for which the maximum stagnation point heat flux and heat load are reached during the descent.
An in-depth CFD investigation is managed for the analysis of the selected undeformed reference shape as illustrated in Fig 3. According to the objectives of the project (see Fig 1), the flight domain investigated is limited to hypersonic and supersonic continuum flow regimes (Mach number between 1.5 and 30). The boundary layer at these conditions may be laminar or turbulent according to the Reynolds number encountered during the flight. 2D-axisymetric Navier-Stokes simulations have been performed at different flight points (depicted in Fig 3) along the heat flux sizing ballistic trajectory. Firstly, four points of interest have been selected in the hypersonic continuum regime:

- the flight point corresponding to the maximum heat flux (around Mach 21);
- the flight point where the maximum pressure is crossed (around Mach 13) for thermal and structural analyses;
- two flight points around the maximum heat flux flight point (at Mach 27 and Mach 8) to have a better assessment of the evolution of the heat flux distribution around the aero-shape to better estimate the heating of the TPS during re-entry in the harshest conditions.

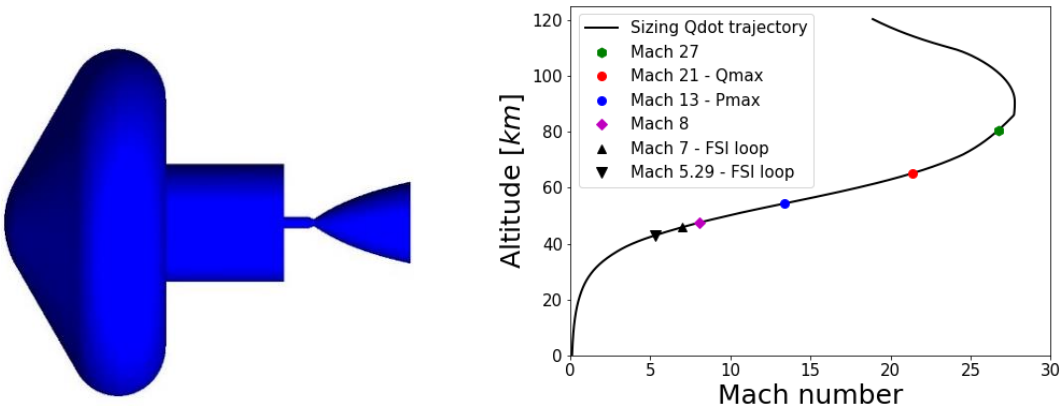

Fig 3. EFESTO-2 aero-shape and the flight points along the *Sizing Heat flux trajectory*.

Then, two flight points are selected in the supersonic regime corresponding to the operating points at DLR's wind tunnel H2K: Mach 7 and Mach 5.29. The objective is to evaluate the deformation levels of the flexible TPS to be tested in the wind tunnel. Finally, in the transonic / subsonic regime three CFD

simulations are selected for Flight Quality Analyses before the parachute deployment: Mach 1.2, Mach 0.9 and Mach 0.7 (not presented in this paper).

2.2. Preliminary aero(thermo)dynamic analysis of the undeformed reference shape

The CFD simulations were performed with the ONERA CFD solver CEDRE considering a chemical non-equilibrium turbulent flow in the shock layer with 17 reactions. More precisely, the computations were done using the Park's 5-species (N_2, O_2, N, O, NO) thermochemical model with 17 reactions [9], Blottner law for viscosity of the species [10], Capitelli database for heat capacity of the species [11], a constant Prandtl number for the determination of their conductivity, and Menter SST-k-ω turbulence model for which the upstream values of the turbulent scalars recommended in the original article are [12, 13]:

$$\frac{V_\infty}{L} < \omega_\infty < 10 \times \frac{V_\infty}{L}, \quad (1)$$

$$\frac{10^{-5} V_\infty^2}{Re_L} < k_\infty < \frac{0.1 V_\infty^2}{Re_L}, \quad (2)$$

where L is "*the approximate length of the computational domain size*". Thus, the values of the upstream turbulent scalars are subject to interpretation and variation. Present CFD results were obtained within the following values $k_\infty = 1\ J/kg$ and $\omega_\infty = 10000\ s^{-1}$ for the turbulent kinetic energy and specific turbulent dissipation respectively. For supersonic and hypersonic regimes, a shock-fitted process to capture the bow shock is used. For the wall, emissivity and catalytic parameters of the upper protection layer have been determined by numerical reconstruction of the DLR's L2K and L3K arc jet tests at characteristic heat flux and heat load of EFESTO re-entry conditions [2] and are considered as the default parameters. However, to complete our analysis and ensure to take sufficient margins, different catalytic conditions are tested: non-catalytic (NC), partially-catalytic (PC) [2] corresponding to the one derived from numerical WTT rebuilding, fully-catalytic (FC) and super-catalytic (SC). Finally, the wall temperature and convective-diffusive heat flux are calculated assuming the radiative equilibrium condition at the wall.

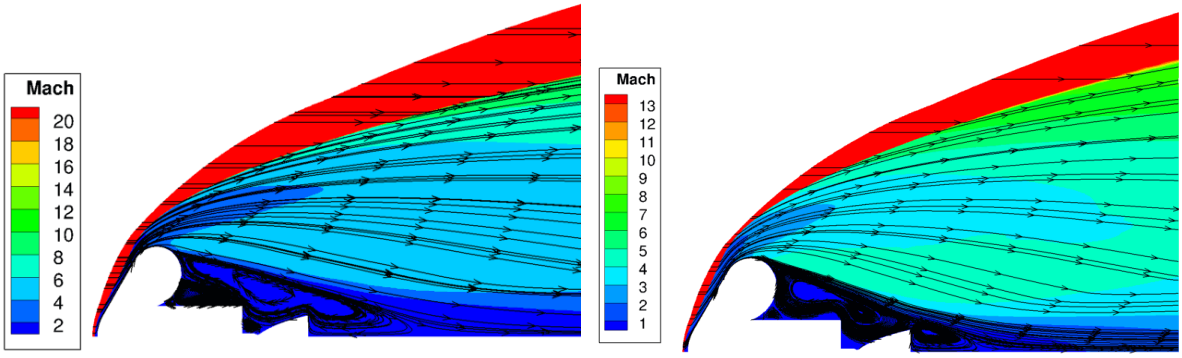

Fig 4. Mach number flow field streamlines considering turbulent flows and partially-catalytic walls - Sizing heat flux trajectory. Left: Maximum heating point (Mach 21). Right: Maximum pressure point (Mach 13).

The CFD computational results for the maximum heating point (Mach 21) and maximum pressure point (Mach 13) are presented in Fig 4. Although the laminar-turbulent transition is purely triggered numerically (no transition model is active, only local boundary layer conditions in terms of turbulent kinetic energy and specific turbulent dissipation may trigger laminar to turbulent flow through given turbulence model), "turbulent" simulations are more representative of the physics than forcing a laminar flow. Accounting for turbulence reduces the recirculation area and exhibits a closer reattachment point of the flow. At 0° angle of attack, there is no flow impingement at the rear of the aero-shape which ensures that no pressure and heat flux peaks would occur on the back-shield. The drag is thus essentially determined by the pressure distribution on the front-shield.

The pressure distributions around the aero-shape for the maximum pressure and the maximum heat flux flight points (Mach 13 and Mach 21 resp.) are displayed in Fig 5. For the maximum pressure point

(Mach 13), stagnation pressure on the front-shield varies from 11000 Pa at the stagnation point to 8900 Pa on the conical part. For the maximum heat flux point (Mach 21), stagnation pressure on the front-shield varies from 6550 Pa at the stagnation point to 5195 Pa on the conical part. Integration of the surface pressure and skin friction leads to assess aerodynamic coefficients, displayed in Fig 5. These latter remain comparable with the ones obtained with "medium fidelity" ARES solution at 0° angle of attack.

The influence of the turbulence on the wall heat flux distribution is pointed out in Fig 6. At Mach 21 (Q_{max} flight point), the numerical laminar-to-turbulent transition occurs at the junction between the cone and the annulus, affecting only the heat flux levels on the annulus but in a limited way. Indeed, maximum heat flux experiment at this location increases from 295 kW/m² (laminar) to 515 kW/m² (turbulent), which is approximately equivalent to the stagnation heat flux value (~515 KW/m²). At Mach 13 (P_{max} flight point), numerical laminar-to-turbulent transition occurs earlier, at the junction between the sphere and the cone. The turbulent boundary layer is then developed all along the cone leading to a major increase of the heat flux levels on both conical part and annulus of the shield.

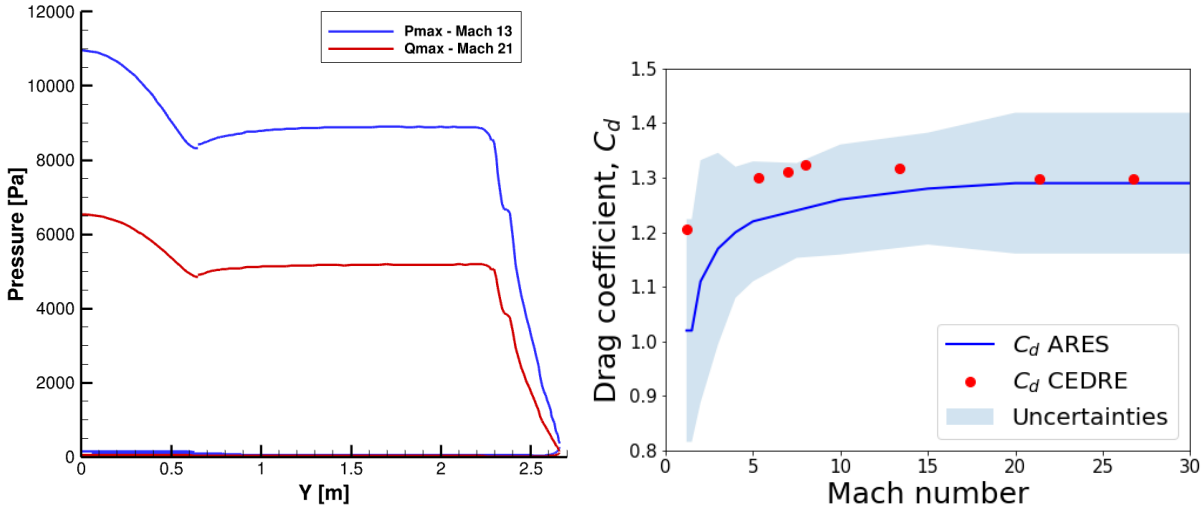

Fig 5. Left: Pressure distributions at the maximum heating point (Mach 21) and at the maximum pressure point (Mach 13). Right: ARES/CEDRE drag coefficient evolution along the entry path corridor - Sizing heat flux trajectory.

The maximal heat flux goes from 180 kW/m² for laminar flow condition to 307 kW/m² for turbulent flow condition; which is higher than the stagnation heat flux (~260 KW/m²). Although turbulent flow has important influence on the wall heat flux and has to be considered for the TPS design process, it is important to remember that: 1) laminar-to-turbulent transition is purely numerical and not linked to experimental evidence of a physical behavior; 2) the turbulence levels in the boundary layer and in the wake depend on the upstream flow turbulence, which is still unknown. Moreover, the initial choice of the values of the turbulent scalars of the numerical turbulence models is subject to interpretation and influences directly the results obtained.

Wall catalycity has a very significant influence on the wall heat flux level, since a factor of two is observed at Mach 21 (Q_{max} flight point) between a super-catalytic and a non-catalytic wall. However, we can notice that the difference between the heat flux obtained for a super-catalytic wall and a partially catalytic wall is very small, with a maximal difference of 1.6 %. This small difference is due to the high value of the atomic recombination parameter for the TPS considered. Even if the differences are small, for design purposes, super-catalytic solutions returning the maximum heat flux distributions have to be considered.

For a better assessment of the heating of the TPS during re-entry in the harshest conditions two extra CFD computations have been performed, one ahead of the maximum heat flux flight point and one below the maximum pressure point, which are respectively at Mach 27 and at Mach 8 (see Fig 3). The evolution of heating levels around the aero-shape in the hypersonic regime is presented in Fig 7. For a

relatively smooth aero-shape and at altitudes where Reynolds numbers are low, at Mach 27 and at Mach 21, such a flow is probably laminar. However, due to uncertainties related to the shape deformation effects and to the lack of knowledge of laminar-to-turbulent transition in the hypersonic regime (since no evident transition model in this regime exists in the literature) we triggered turbulence at all altitudes to propose an additional margin on heat flux levels. We notice that, at Mach 27, computed flow maintained fully laminar along the front-shield due to the relatively low dynamic pressure at this altitude. Finally, heat flux distribution for the maximum heating point, at Mach 21, wraps all other distributions, which can be considered as the most critical situation in terms of heat flux levels for the design of the flexible TPS.

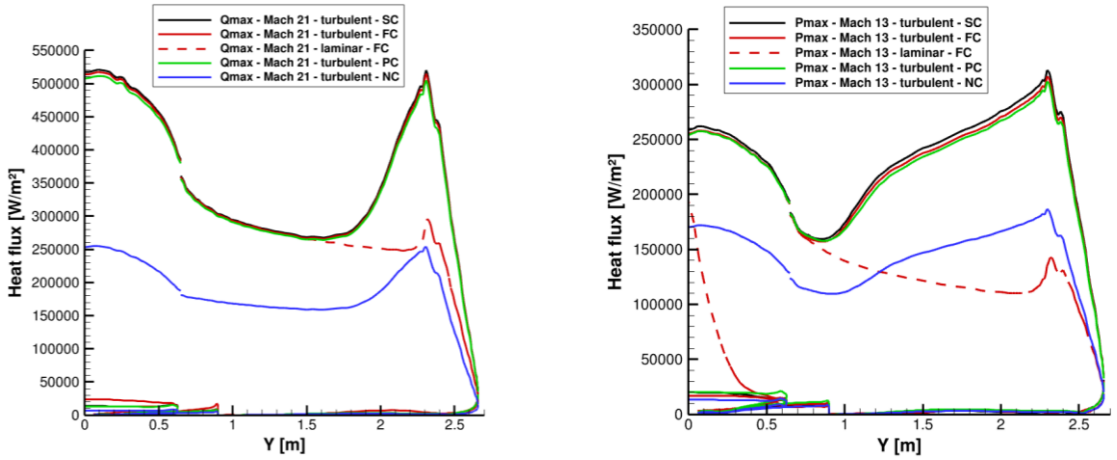

Fig 6. Heat flux distributions - Sizing heat flux trajectory. Left: Maximum heating point (Mach 21). Right: Maximum pressure point (Mach 13).

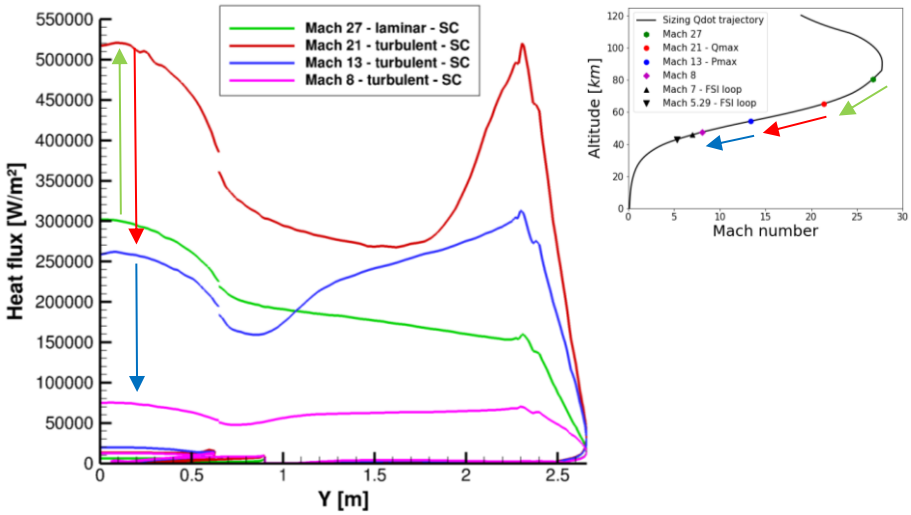

Fig 7. Evolution of the heat flux distributions for Mach 27, 21, 13, 8 - Sizing heat flux trajectory.

2.3. Fluid structure interaction analysis

Knowing the pressure distributions at different flight points of the trajectory, a Fluid Structure Interaction (FSI) investigation is done to evaluate the impact of the shape deformation on both aerodynamic drag and aerothermal loads. Further, the FSI simulations allowed identification of the deformed shape to be replicated for WTT tests.

Methodology

Numerically, the coupling between fluid dynamic (CFD code) and structural mechanics (FEM code) can be either strong or weak. The strong/tight interaction claims for a mathematical model where

aerodynamic/aerothermodynamic and structural aspects are strongly and intrinsically cross-correlated. On the contrary, the weak/loose coupling is based upon a continuous exchange of inputs/outputs between the solvers associated to the two disciplines. In EFESTO-2, because of the quasi-static aeroelastic nature of the problem the weak/loose coupling, depicted in Fig 8, is chosen. Basically, the loop is triggered by the CFD by obtaining the flow field around an initial undeformed shape to get the wall pressure distribution. Secondly, the pressure pattern is applied as input to the structural FEM code on the shape itself to get, through a static-load analysis, the subsequent deformed shape. Then, the deformed shape is passed again to the CFD solver to determine the flow field around a deformed geometry, which brings to a new pressure pattern to be passed again to the FEM solver for a further iteration of FSI. The loop goes on until the convergence is reached. For that task, the chosen modelling tools are:

- The ONERA CFD solver CEDRE for aerodynamic/aerothermodynamic, since this tool is well established and widely used, not only for the EFESTO projects, but also for many other past and current projects.
- The commercial FEM code Abaqus at premises of CIRA/Subco already used in EFESTO-1. For these simulations, the material properties of the IS main elements determined in EFESTO-1 are used.

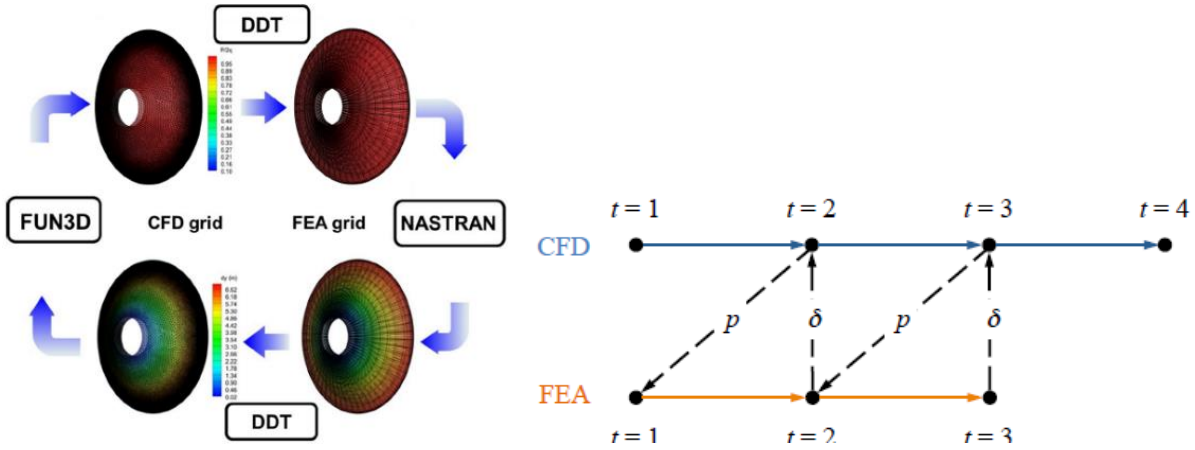

Fig 8. Fluid Structure Interaction logic.

Convergence criterion

During the FSI loops different outcomes are exchanged between CEDRE (CFD) and Abaqus (FEM): the pressure level on the conical region of the shape, the displacement or deformation of the shape, and the drag/axial coefficient (C_A) of the shape.
The computation is considered as converged when the delta or change of the absolute value of any key parameter, from an iteration to the next one, is such to exhibit a negligible difference.

FSI meaningful flight condition

Based on an iterated discussion within the technical team of the EFESTO-2 project, it has been decided to shape the FSI loop according to the following logic:

- focus the investigation on the critical trajectory points where the deformation is expected to produce a meaningful yet significant effect,
- maximize the synergy with the wind-tunnel test effort that will be carried out.

Thus, the flight points are chosen in such a way that, firstly, the critical conditions are sizing for the system itself, i.e. where the deformation has the most significant impact (corresponding to the maximum pressure and heat flux flight points); and secondly, to stick as much as possible with the Mach ranges replicable in the WTT facilities: the hypersonic wind-tunnel H2K and the supersonic wind-tunnel TMK. H2K and TMK being able to work in the Mach range of [5.3 to 11.2] and [1.2 to 5.6],

respectively, We finally selected the four following flight points, depicted in **Erreur ! Source du renvoi introuvable.**Fig 3:

- Mach 21.35, corresponding to the max heat flux flight point,
- Match 13, corresponding to the max pressure flight point (not presented in this article),
- Mach 7 (see section 2.4) for the H2K wind tunnel,
- and Mach 3.5 for the TMK wind tunnel.

The pressure inside the conical section of the inflatable structure is critical for the deformation. The closer the internal pressure is to the external pressure, the less the wall deforms. The TPS is designed to survive to the most sizing aerothermal environment. However, since the thermal protection system is dimensioned with respect to the distribution of the heat flux along the undeformed heat shield, the greater is the deformation at this condition, the more unpredictable will be the heat-flux distribution. So, the required inflation pressure in the conical volume to ensure minimization of deformation should be exactly in the order of 5 kPa, corresponding to the mean pressure encountered on the conical part at Mach 21 (Fig 9), which is the maximum heat flux flight point.
Since for the flight points at Mach 13, 7 and 3.5, the external pressure is higher than 5 kPa (Fig 9), the degree of the wall deformation has to be determined. At Mach 3.5, a negligible deformation is expected. Since the case at Mach 7 is the only one replicable in the H2K wind tunnel, only the result of the FSI loop for this condition is presented in next section.

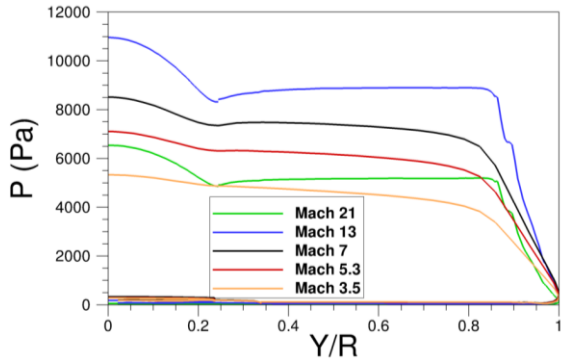

Fig 9. Pressure distribution at the wall for various flight points along the *sizing heat flux trajectory*.

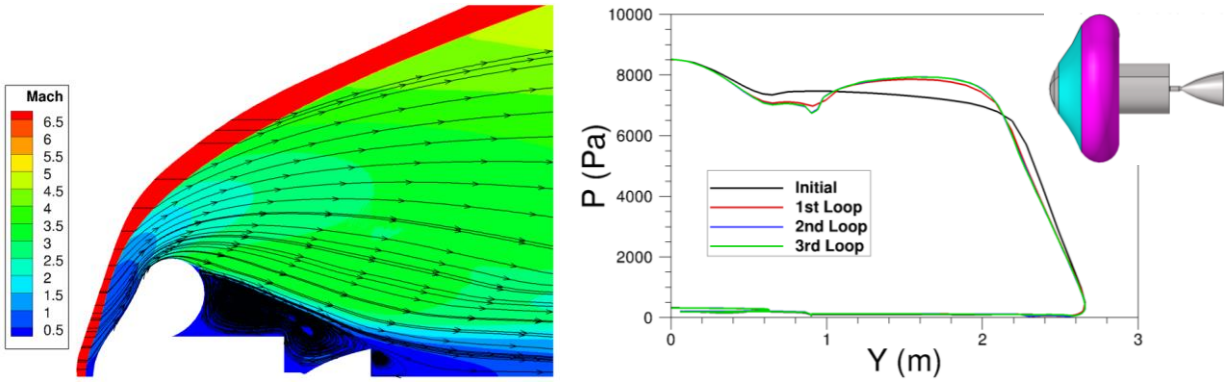

Fig 10. Mach field around the last deformed shape (left) and pressure distribution evolution (right).

2.4. CFD investigation for the Mach 7 case

Starting from the undeformed condition of the shape at Mach 7 (see Fig 3), pressure pattern was first obtained by a CFD computation and then applied to the undeformed shape in the FEM to get the first deformation pattern; the procedure is repeated until convergence. Fig 10 shows the Mach field around the converged deformed body and the evolution of the external wall pressure distribution for the different (un)deformed shapes at Mach 7. In this case, four iterations and three deformed shapes were

necessary to achieve convergence, as illustrated in Table 1. We notice that the pressure distribution on the flexible conical part is slightly modified by the deformation due to dynamic pressure: the peak pressure is increased by 6.56 % while aerodynamic drag coefficient is increased by 1 %. The converged deformed shape was adopted to be tested in the H2K wind tunnel.

Table 1. Comparison of shape evolution for the Mach 7 case.

KPI evolution (abs)	Stage 0	Stage 1	Stage 2	Stage 3
Shape	undeformed	deformed 1	deformed 2	deformed 3
Displacement [mm]	---	-49	-57	-58.4
Peak pressure [kPa]	7.46	7.86	7.94	7.95
C_A (or C_D @ 0 deg AoA, Mach 7 [-]	1.3120	1.3212	1.3240	1.3244

*On the conical region

3. WTT-CFD Cross-correlation

3.1. Preliminary simulations for wind tunnel test (WTT) preparation

Of significant importance in the frame of the project is the implementation of a wind-tunnel test campaign aiming at investigating aerodynamics and flying qualities of capsule-like bodies in both deformed and undeformed conditions. Two DLR-Cologne facilities are involved, H2K facility for static tests in hypersonic Mach range [5.3, 7]; and TMK facility (Fig 11) for static and dynamic tests in supersonic Mach range [1.4-4]. According to the FSI loop results only the undeformed shape will be tested in TMK while deformed and undeformed shape will be tested in H2K wind tunnel. So, two different sub-scaled models of both, deformed and undeformed shapes, have been designed and manufactured for that purpose (see Fig 12). Scaled models of 2% in H2K and 1.5% in TMK have been designed.

Fig 11. H2K (left) and TMK facility at DLR-Cologne (right) [7].

In H2K, we can try to reproduce the upstream dynamic pressure or Reynolds number while in TMK, only Reynolds number can be reproduced. However, in H2K, some limitations are encountered, the equivalent upstream flow conditions cannot always be reproduced. For example, at Mach 5.3, the dynamic pressure of the flight cannot be reproduced (see Table 2). The upstream flow conditions in flight and wind tunnel "flight equivalent" conditions (dynamic pressure and Reynolds number) are summarized in Table 2 for the flight points at Mach 7 and 5.3.

To prepare the test campaigns in H2K and to define the best strategy – i.e. choose to reproduce the upstream dynamic pressure and/or the Reynolds number of selected flight points during the test – preliminary CFD simulations are carried out. Since only the Reynolds number can be reproduce in TMK, there is no choice to do. So, no preliminary simulations have been performed for TMK WTT.

For H2K WTT experiments, several 2D-axisymetric CFD numerical simulations have been performed: 1) in flight conditions, with the 1:1 scale geometry; 2) under equivalent upstream flow conditions with scaled geometries.

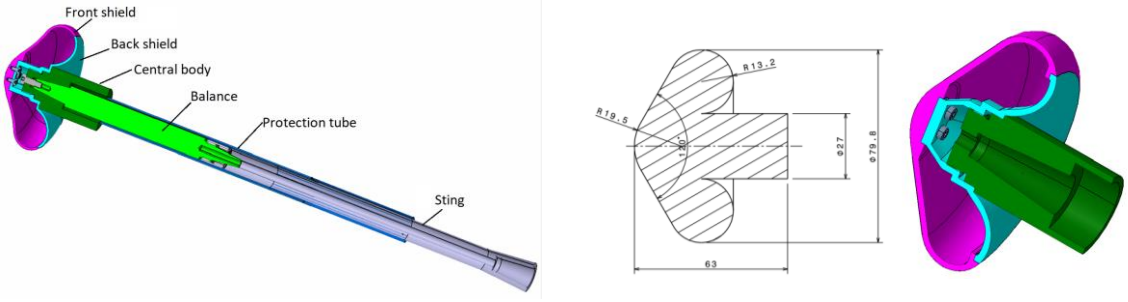

Fig 12. The wind tunnel model of the deformed shape for H2K WTT (left) and undeformed shape for TMK WTT (right) [7].

Table 2. Flight and H2K wind tunnel test conditions.

	Mach 7			Mach 5.29		
	Flight condition	**Dynamic pressure eq.**	**Reynolds eq.**	**Flight condition**	**Dynamic pressure eq.**	**Reynolds eq.**
Altitude (km)	45.91	-	-	42.99	-	-
Pressure (Pa)	132.83	132.8	746.7	193.24	268.2	1281.4
Temperature (K)	266.68	50	58.3	258.61	62	63.5
Velocity (m/s)	2291.4	992.4	1072	1706.56	836.4	846.6

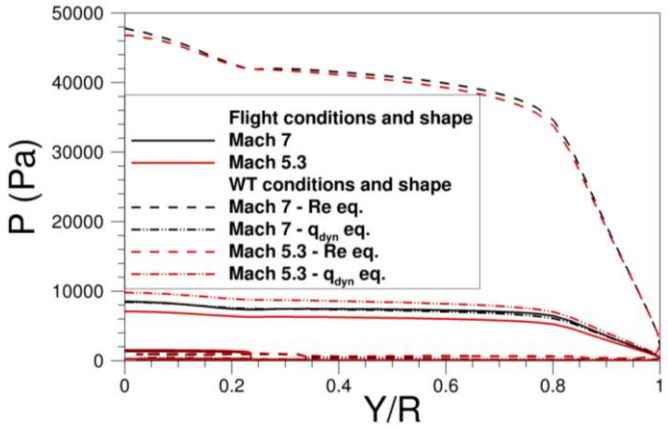

Fig 13. Pressure distribution calculated with CFD code CEDRE at both Mach 7 and 5.3 in flight conditions assuming scale 1:1 shape and in H2K conditions with the scaled model.

As illustrated in Fig 13, at Mach 7, pressure distribution along the heat shield is equal to the one obtained in flight when upstream dynamic pressure is reproduced in the wind tunnel test. A discrepancy exists between the pressure distribution corresponding to flight conditions and equivalent dynamic pressure (q_{dyn}) at Mach 5.3, since the equivalent dynamic pressure cannot be strictly reproduced in H2K for this condition. Whatever the flight point, reproducing the upstream Reynolds number leads to important pressure distribution levels along the shield and far from the pressure encountered in flight. The axial force coefficients C_A calculated with CEDRE (CFD) for in flight and H2K WTT conditions at Mach 7 and 5.3 and 0° angle of attack are given in Table 3. We can notice some differences between the axial force coefficients obtained for WTT conditions and the one calculated with the flight conditions whatever the Mach number.

In conclusion, the consortium decided that the H2K WTT will be carried out under each of the following three conditions: Reynolds equivalent, dynamic pressure equivalent and intermediate conditions between the two previous ones.

Table 3. Axial force coefficient C_A obtained by CFD simulations in flight and in H2K wind tunnel test (WTT) conditions – undeformed shape – Mach 7 and 5.3 at 0° angle of attack.

	Mach 7	Mach 5.3
Flight conditions	1.31	1.30
WTT conditions, dyn. Pressure eq.	1.28	1.27
WTT conditions, Re eq.	1.28	1.28

Table 4. Comparison between CFD and experimental axial force coefficients for TMK wind tunnel test on undeformed shape (0° angle of attack).

Test Nr.	Ma	C_A CFD	C_A Exp	Relative Err. (%)
1	1.82	1.3548	1.2941	4.69
2	1.99	1.3392	1.3018	2.88
3	1.49	1.3546	1.2538	8.04
4	1.45	1.3589	1.2485	8.84
5	1.41	1.3500	1.2332	9.47
7	2.53	1.3246	1.3155	0.69
8	3.01	1.3131	1.33	1.27
9	3.5	1.3048	1.3158	0.84
10	3.96	1.3056	1.2914	1.10

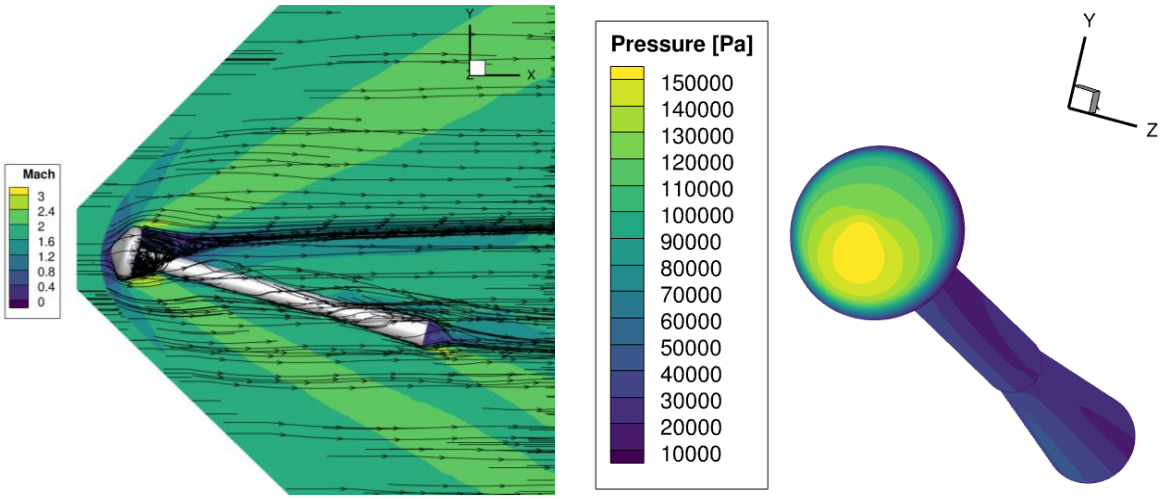

Fig 14. Mach flow field (left) and pressure distribution (right) at Mach 2 and 15° of AoA, corresponding to the case #2 of the TMK test campaign.

3.2. Numerical rebuilding of the WTT experiments

The test campaign having first been carried out in TMK and the H2K tests being finished not long ago, only the numerical rebuilding of the TMK wind tunnel test are presented in this paper.

The turbulent CFD simulations were performed with the ONERA CFD solver CEDRE considering air as a perfect gas and using the Menter SST-k-ω turbulence model. The air viscosity is calculated using the Sutherland law and a constant Prandtl number is taken for the air conductivity.

Preliminary comparison between CFD and experimental results for TMK wind tunnel test on undeformed shape at 0 degree angle of attack are presented in Table 4. The relative error between numerical and experimental data varies from 0.6% to 9.5%. The most important relative errors are obtained for the

lowest Mach number (1.41; 1.45; 1.49). The relative error decreases while Mach number increases. These data are still subject of the current analysis.
3D simulations with angle of attack (AoA) of 5°, 10° and 15° are under progress as illustrated in Fig 14.

4. Conclusion

Evaluation of the IHS deformation influence on the aerodynamic coefficients and the wall heat flux is a key point of the design of the mission and the heat shield itself. To reach this objective ground test campaigns and numerical rebuilding are necessary steps. This paper presents pre-numerical investigation allowing the definition of the test articles and the test campaigns, as well as post-numerical rebuilding with numerical-experimental cross-correlation to improve the predictive capability at materials, structural and aerothermodynamics level. These studies are conducted in the frame of the EFESTO-2 project and still ongoing. The EFESTO-2 project receives funding from the European Union under the Horizon Europe research and innovation programs, (grant agreement No.101081104). For further information, please visit the project website at: http://www.efesto-project.eu.

References

1. Guidotti, G. et al.: EFESTO 1 & 2: European Achievements And Expected Advancements In Inflatable Heat Shields For Mars And Earth Re-Entry Applications. In: 20th International Planetary Probe Workshop – Marseille, France, 2023.
2. Schleutker, T. et al.: Flexible TPS design and testing for advanced European re-entry system based on inflatable heat shield for EFESTO project. In: 2nd International Conference on Flight Vehicles, Aerothermodynamics and Re-entry Missions & Engineering - Heilbronn, Germany, 2022.
3. Gardi, R. et al.: Design development and testing of the Inflatable Structure and its Demonstrator for the EFESTO project. In: 2nd International Conference on Flight Vehicles, Aerothermodynamics and Re-entry Missions & Engineering, Heilbronn, Germany, 2022.
4. Governale, G. et al.: Advanced European Re-Entry System Based on Inflatable Heat Shields EFESTO-2 project overview. In: 74th International Astronautical Congress (IAC), Baku, Azerbaijan, 2-6 October 2023.
5. Guidotti, G. et al.: EFESTO-2: European Flexible Heat Shields Advanced TPS Design and Tests for Future In-Orbit Demonstration – 2. In: Aerospace Europe Conference 2023 – 10th EUCASS – 9th CEAS - Lausanne, Switzerland, 2023.
6. Guidotti et al.: Inflatable Heat Shields solutions for hypersonic re-entry applications: the European Commission EFESTO-2 project. In: 3rd International Conference on High-Speed Vehicle Science Technology (HiSST), Busan, Korea, 2024.
7. Zhai, J. et al.: Experimental aeroshape characterization of an Inflatable Heat Shield re-entry vehicle in the EFESTO-2 project. In: 3rd International Conference on High-Speed Vehicle Science Technology (HiSST), Busan, Korea, 2024.
8. Gardi, R. et al.: Modelling, simulation and testing of inflatable structures applied to re-entry in the EFESTO-2 project. In: 3rd International Conference on High-Speed Vehicle Science Technology (HiSST), Busan, Korea, 2024.
9. Park C.: Review of chemical-kinetic problems of future NASA missions, I: Earth entries. Journal of Thermophysics and Heat Transfer, 7(3), 1993.
10. Blottner, F et al.: Chemically Reacting Viscous Flow Program for Multi-Component Gas Maixtures, Tech. Rep., SC-RR-70-754, Sandia Laboratories, Albuquerque, New Mexico, 1971.
11. Capitelli, M. et al.: Tables of Internal Partition Functions and Thermodynamic Properties of High-Temperature Mars-Atmosphere Species from 50K to 50000K. Tech. Rep., ESA STR-246, ESA Publications Division, 2005.
12. Menter, F. R.: Improved Two-Equation k-omega Turbulence Models for Aerodynamic Flows. NASA TM 103975, 1992.
13. Menter, F. R.: Two-Equation Eddy-Viscosity Turbulence Models for Engineering Applications. AIAA Journal, Vol. 32, No. 8, pp. 1598-1605, 1994.